Dye-sensitized solar cells fabricated using ZnO:Cu thin films and dye extracted from *Hypericum perforatum L.* flowers

F. Göde[a,*], N. Balpınar[b]
[a]*Department of Physics, Faculty of Arts and Sciences, Burdur Mehmet Akif Ersoy University, 15030 Burdur, Turkey*
[b]*Department of Biology, Faculty of Arts and Sciences, Burdur Mehmet Akif Ersoy University, 15030 Burdur, Turkey*

Dye-sensitized solar cells (DSSC) were designed utilizing pure and copper-doped zinc oxide (ZnO:Cu) nanoparticles and the dye extracted from dried *Hypericum perforatum L.* (*H. perforatum*) flowers. The ZnO:Cu thin films were grown using the successive ionic layer adsorption and reaction (SILAR) method on tin-doped indium oxide-coated (ITO) glass substrates at 85 °C. Regarding the molar ratio of Cu ions to Zn ions, Cu had a doping concentration of 0.5%, 1%, and 2%. The crystalline nature, morphological, compositional, and optical properties of the synthesized ZnO:Cu thin films were studied using an X-ray diffractometer (XRD), a scanning electron microscope (SEM), energy dispersive x-ray spectrometry (EDS), UV-vis spectroscopy, and Fourier transformation infrared (FTIR) spectroscopy. The SEM results indicated the formation of a porous structure on the surface of ZnO:Cu thin films, which provided more active sites for dye molecules and electrolyte ions. A DSSC, produced by using a pure ZnO thin film, showed a current density (J_{sc}) of 7.66 mA/cm^2 with an open-circuit voltage (V_{oc}) of 0.98 V and an overall efficiency (η) of 2.47%.

(Received December 19, 2022; Accepted March 16, 2023)

Keywords: Cu-doped ZnO, SILAR method, *Hypericum perforatum L.*, Dye-sensitized solar cells

1. Introduction

In recent years, solar power has gained prominence among alternative energy sources because it is clean and renewable. Solar energy demand increases day by day in parallel with the world's increasing demand and consumption. Such a demand motivates the studies of developing photovoltaic (PV) systems. Many types of solar cells have been designed to harness this kind of energy. The dye-sensitized solar cells (DSSC) are known as third-generation photovoltaic solar cells regarding their relatively high conversion efficiency, low production cost, easy and environment-friendly fabrication, ability to perform in indoor as well as in diffused light [1-5].

Solar energy is converted into electrical energy via a DSSC device, which uses dye molecules to produce electricity according to the principle of sensitization of dye molecules into the semiconductor electrode material. The dye is light-sensitive and used as a light-sensitization material in DSSC. The dye molecules absorbing the light excite the electron from the HOMO level to the LUMO level and provide electron injection through the conduction band of the metal oxide semiconductor (MOS) [6]. The anode (working electrode) of DSSC has a thick layer of MOS thin film that constitutes a large surface for the attack of dye molecules. The MOS takes electrons from the dye molecule and transfers them to the photocathode (counter electrode) [7]. For this reason, electron transfer is crucial for DSSC, and it depends on the photoanode to a great extent.

Among many MOS, ZnO is assumed to be the best alternative material for photoanodes instead of TiO_2 and SnO_2 due to being a non-toxic, low-cost, and eco-friendly material with a direct optical bandgap of 3.37 eV and an exciton binding energy of 60 meV at room temperature [8]. Besides, pigments (chlorophyll, carotenoid, anthocyanin, lutein, rutin, and betalain) extracted

* Corresponding author: ftmgode@gmail.com
https://doi.org/10.15251/DJNB.2023.181.389

from various plant parts, such as flowers, fruits, and leaves, are known as sensitizers in DSSC. Numerous studies examine some MOS electrodes and dyes to develop the energy conversion efficiency of DSSC [9]. However, improving the cell performance of the current DSSC is not clear and needs in-depth study.

ZnO thin films can be synthesized using different techniques, such as wet precipitation [10], sol gel [11], chemical bath deposition (CBD) [12], hydrothermal [13], and successive ionic layer adsorption and reaction (SILAR) [14]. Among these methods, SILAR is simple, inexpensive, and reproducible. In this study, the SILAR method was used to synthesize pure and copper-doped ZnO:Cu thin films. The synthesized thin films were used as photoanodes in the DSSC. *Hypericum perforatum* L. (*H. perforatum*) dye extract was used as a sensitizer in the DSSC. To the best of the authors' knowledge, production of DSSC using this sensitizer with ZnO:Cu nanoparticles is reported for the first time. The study also compares the performance of some DSSC devices.

Hypericum is a genus that belongs to the *Hypericaceae* family and is European in origin. This genus, which has a wide distribution on every continent except Antarctica, includes about 500 species [15,16]. The genus is represented by 107 taxa in 20 sections in Turkey, 46% of which are endemic [17]. *H. perforatum* is a perennial plant that prefers dry habitats and has an upright stem that grows 10 to 110 cm tall. Occasionally, the stem may come out horizontally, but it subsequently rises upward. The body of the plant is more branched at the tip. Because of their many medicinal properties, *Hypericum* species have been widely utilized in traditional treatment, especially in the treatment of depression, all over the world since ancient times [18]. In particular, *H. perforatum* is known as "St. John's wort" and it is the most researched species in the world due to its economic importance in the herbal industry [19]. The species, which has a wide distribution in Turkey, especially in Mediterranean phytogeographic region, is also extremely popular among the people and is known by names such as binbirdelikotu, mayasılotu, sarı kantaron, kanotu, yaraotu and kuzukıran [20].

2. Material and methods

2.1. General

Zinc chloride [($ZnCl_2$); MA = 136.30 g/mol; ACS Reag Ph Eur], copper nitrate [($Cu(NO_3)_2H_2O$); MA = 241.60 g/mol; 99.5% purity], hydrogen peroxide [(H_2O_2); d = 1.13 g/cm^3; 35% purity], ammonium [(NH_4); Ph Eur, BP grade; 25% purity], iodine [(I_2); MA = 253.8 g/mol; ACS, ISO, Reag. Ph Eur grade] and acetonitrile [(C_2H_3N); Reag. Ph Eur grade; MA = 41.05 g/mol] were purchased from Merck. Ultrapure water used in the present study had a resistivity of 18.2 M Ω cm. Potassium iodide [(KI); MA = 166.01 g/mol; PH. Eur. BP grade, USP; 99–100,5% purity] was bought from Balmumcu, Turkey. Glass substrates coated with tin-doped indium oxide (ITO) for the study had a sheet resistance of ≤ 10 Ω/sq and dimensions of 76 × 26 × 1 mm^3.

2.2. Instrumentation

The ZnO:Cu thin films were crystallographically analyzed on a Bruker D8 advanced X-ray diffractometer (XRD) between 20° and 70° using CuKa radiation (wavelength 1.5406). A FEI Quanta 250 FEG scanning electron microscope (SEM) and an energy dispersive X-ray spectrometer (EDS) attached to the SEM were used to determine the surface morphologies of the produced films and the elemental composition of them, respectively. Transmittance and optical absorption spectra were measured using a PG-T60 spectrophotometer in the 300–1100 nm wavelength range. In order to get information regarding the functional groups found at the surface of the ZnO:Cu thin films and inside the extracted *H. perforatum* dye, a Fourier transform infrared (FTIR) spectrometer (Perkin Elmer Fronter) was used at room temperature within the range of 700 cm^{-1} to 4000 cm^{-1}. The thicknesses of the ZnO:Cu thin films were determined using cross-sectional SEM images. Besides, in order to determine the power conversion efficiency of the fabricated DSSC under the illumination of a 7 W LED lamp, current voltage (I-V) characteristics were carried out utilizing a Keithley 2400 Source Measurement Unit.

2.3. Synthesis of the ZnO:Cu thin films

The cleanliness of the ITO substrates made them susceptible to film deposition. For this reason, the ITO substrates were cleaned using washing liquid, boiled in ultrapure water, and waited in ethanol, ultrapure water, and acetone for 15 minutes sequentially before deposition. Ammonium hydroxide (NH_4OH), bath temperature, reaction time, and rinsing time were optimized to get crystalline film structure by the SILAR method.

In order to deposit the ZnO thin film, the ITO substrate was dipped in the cation precursor solution, containing 0.1 M $ZnCl_2$ and 9.96 M NH_4OH, for 30 s, followed by submerging into the anion solution, containing 1% H_2O_2, for another 30 s. The SILAR deposition was maintained under ambient pressure at 80 °C. The SILAR steps were repeated 20 times to produce pure ZnO thin film on an ITO substrate. Utilizing the same procedure, the ZnO:Cu thin films were also deposited. The doping concentrations of Cu were 0.5%, 1%, and 2% (regarding the molar percentage of Cu ions to Zn ions). The produced films were annealed at 450 °C for 1 hour in order to remove organic residues.

2.4. Extraction of dye-sensitizer solvent from the dried H. perforatum flowers

In order to extract dye from dried *H. perforatum* flowers, the pulverized plant was soaked in a suitable solvent. Because it increased the performance of DSSC, the solvent chosen for this purpose was ethanol. *H. perforatum* flowers were bought from the local market and carefully washed under running tap water to remove the foreign matter. After this process, the flowers were dried out in the shade for one week at room temperature. Then, the flowers were pestled using a mortar to obtain a coarse powder. Approximately 20 g of the powdered flowers of *H. perforatum* were dissolved in 100 ml of ethanol, and the resulting solution was continuously and gently stirred for 24 h. Next, the solution was filtered using filter paper (whatman) to obtain a clean extract of *H. perforatum*. To prevent the dye material from being exposed to light, it was covered with aluminum foil and kept at 4 °C for use at a later time.

2.5. Preparation of electrolyte solution

In the present study, a common electrolyte (I^-/I_3^-) in an organic solvent (acetonitrile) was used in order to improve efficiency in DSSC. The solution was made by dissolving 0.3 M of potassium iodide (KI) in aqueous solution, and 0.03 M of iodine (I_2) in acetonitrile. Then, it was taken in a 1:1 ratio (by volume) from both solutions.

2.6. Fabrication of DSSC

First, the ZnO:Cu thin films were synthesized onto the ITO substrates with different molar concentrations of Cu (0%, 0.5%, 1%, and 2%) using the SILAR method. The films were then immersed in a *H. perforatum* dye solution for 12 hours at room temperature in the dark. The color of the present films turns into a root green after absorbing the *H. perforatum* dye. Third, the glass/ITO/ZnO:Cu/*H. perforatum* structure (photoanode) was clipped with another ITO substrate used as a photocatode (counter electrode) to form a sandwich-type structure. Finally, the redox electrolyte (I^-/I_3^-) was injected into the gap between the photoanode (working electrode) and counter electrode. Silver contacts were made onto ITO substrates by hand using silver paste. The solar cell parameters, such as efficiency (η), fill factor (FF), open-circuit voltage (V_{oc}) and short-circuit current density (J_{SC}) were determined as reported in [21,22].

3. Results and discussion

3.1. X-ray diffraction analysis of the ZnO:Cu thin films

The XRD pattern of ZnO:Cu thin films deposited at different copper concentrations (in molar at 0%, 0.5%, 1%, and 2%) can be seen in Fig. 1. The existence of a ZnO single phase with a hexagonal wurtzite structure is indicated by the XRD patterns of the films. Diffraction peaks at 32.12°, 34.78°, 36.71°, 45.70°, 57.00°, and 63.45° correspond to the (100), (002), (101), (102), (110), and (103) planes of ZnO, respectively (JCPDS card no. 001-1136; = 3.24; c = 5.17). The intensities of the diffraction peaks observed at 32.12°, 34.78°, 36.71°, 45.70°, 57.00°, and 63.45°

correspond to the (100), (002), (101), (102), (110), and (103) planes of ZnO, respectively (JCPDS card no. 001-1136; = 3.24; c = 5.17). As can be seen, the intensity of the diffraction peak observed at 2θ = 32.12° corresponds to the (001) plane and decreases with the increasing Cu doping concentration of 0.5% and disappears with more Cu doping. The lower intensity peak observed at 2θ = 45.70° corresponds to the (102) plane, on the other hand, increases slightly in intensity with increasing Cu doping. Additionally, all ZnO:Cu thin films show the ITO peaks coming from the substrate [21,22]. The intensity of these peaks becomes more apparent when the doping concentration of Cu increases in the ZnO thin film.

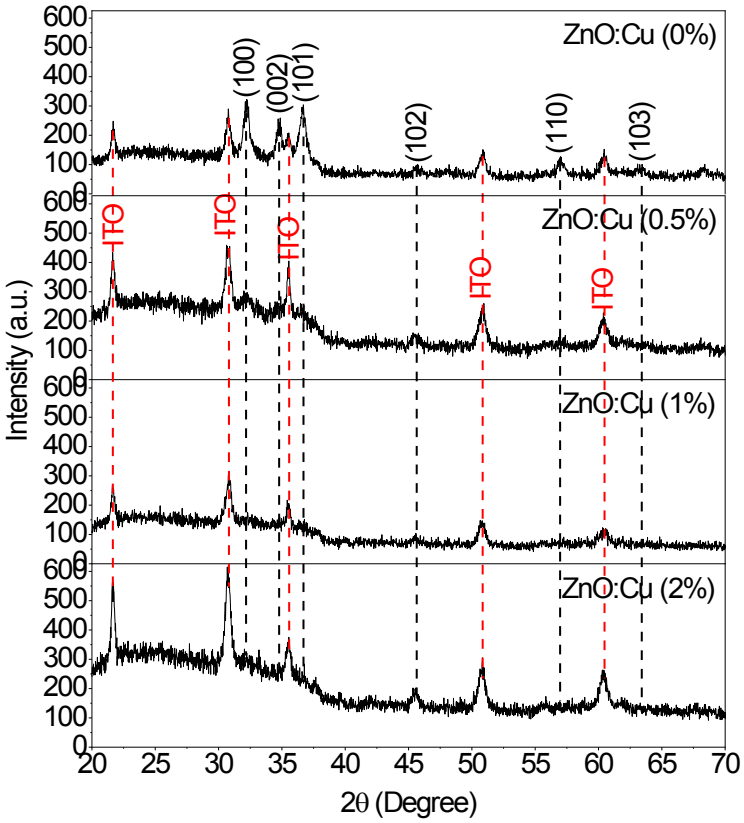

Fig. 1. X-ray diffraction pattern of the ZnO:Cu thin films.

The lattice constants (a and c) re obtained from the XRD analysis using the hexagonal structure's following relationship:

$$\frac{1}{d_{hkl}^2} = \frac{4}{3}\left[\frac{h^2 + hk + k^2}{a^2}\right] + \frac{l^2}{c^2} \tag{1}$$

where h, k, l are miller indices, and d_{hkl} is distance between the planes. The lattice parameters a and c calculated for pure ZnO thin films are 3.21 Å and 5.15 Å, respectively. They are very consistent with the reported values [23]. The comparison of the experimental and standard structural parameters of the ZnO:Cu thin films is listed in Table 1.

Table 1. Structural parameters of the ZnO:Cu thin films.

Material	Observed values		Standard values		a (Å)	c (Å)	(hkl)
	2θ (°)	d (Å)	2θ (°)	d (Å)			
Pure ZnO	32.12	2.784	31.82	2.810	3.21	5.15	(100)
	34.78	2.576	34.33	2.610			(002)
	36.71	2.446	36.49	2.460			(101)
	45.70	1.983	47.56	1.910			(102)
	57.00	1.614	57.16	1.610			(110)
	63.45	1.464	63.20	1.470			(103)
ZnO:Cu 0.5%	32.06	2.789	31.82	2.810	3.22	5.51	(100)
	45.51	1.991	47.56	1.910			(102)
ZnO:Cu 1%	45.57	1.988	47.56	1.910	-	-	(102)
ZnO:Cu 2%	45.59	1.987	47.56	1.910	-	-	(102)

3.2. Scanning electron microscope (SEM) micrographs of the ZnO:Cu thin films

The study of the morphological characteristics of the ZnO:Cu thin films gives important details regarding the size, shape, and growth mechanism of the particles. The surface morphologies of the ZnO:Cu thin films are taken at 50.000× and 100.000× magnifications. It is clear that the synthesized ZnO nanoparticles have a mixing of spheroid-like and rod-like particles with remarkable vacant space in between (see Figs. 2(a-h)). With an increasing Cu concentration, this morphology starts to deteriorate slightly and finally turns into spherical grains (see Figs. 2(e) and (j)). Similar results regarding the surface morphology of ZnO thin film can be observed in the literature [24].

In order to determine the film thicknesses, cross-sectional SEM morphologies of the ZnO:Cu thin films have been taken (see Figs. 2(k-o)). These figures and Table 2 show that as Cu doping increased, film thickness decreased from approximately 1619 to 615 nm.

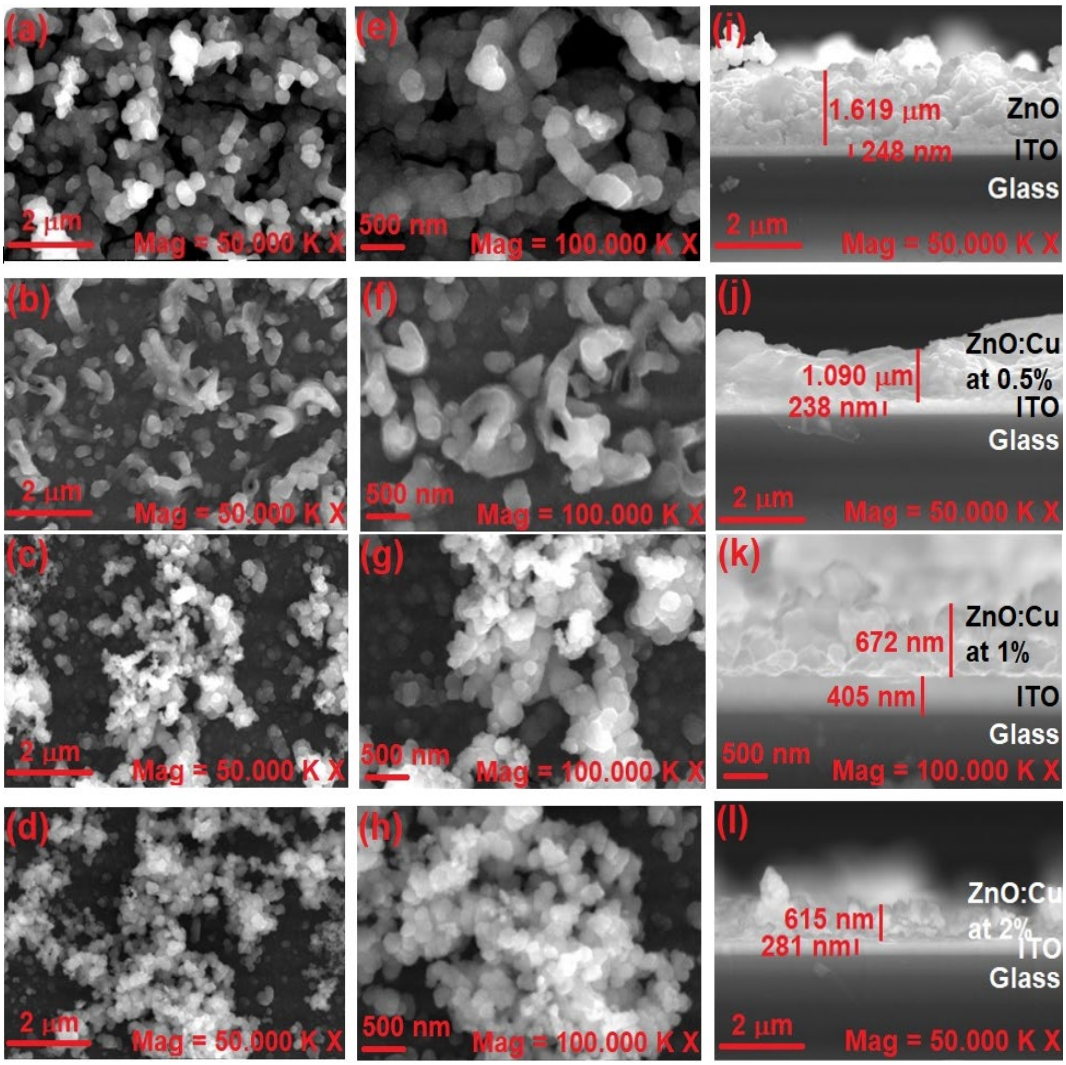

Fig. 2. The SEM micrographs and cross sectional SEM images of the ZnO:Cu thin films with different Cu doping (a,e and i) Cu at 0%, (b, f and j) Cu at 0.5%, (e, g and k) Cu at 1% and (d, h and l) Cu at 2%.

3.3. Energy-dispersive X-ray (EDS) spectra of the ZnO:Cu thin films

The chemical composition of the ZnO:Cu thin films was analyzed using EDS measurements shown in Fig. 3, and the results listed in Table 2. This table shows that the analysis based on EDS indicates the presence of O, Zn, In, and Cu elements in the present films. It was observed that the atomic percentage of the films showed an excess of oxygen. The underlying reason is that we used the aqueous solution method [25]. We consider that excess oxygen comes from ultrapure water.

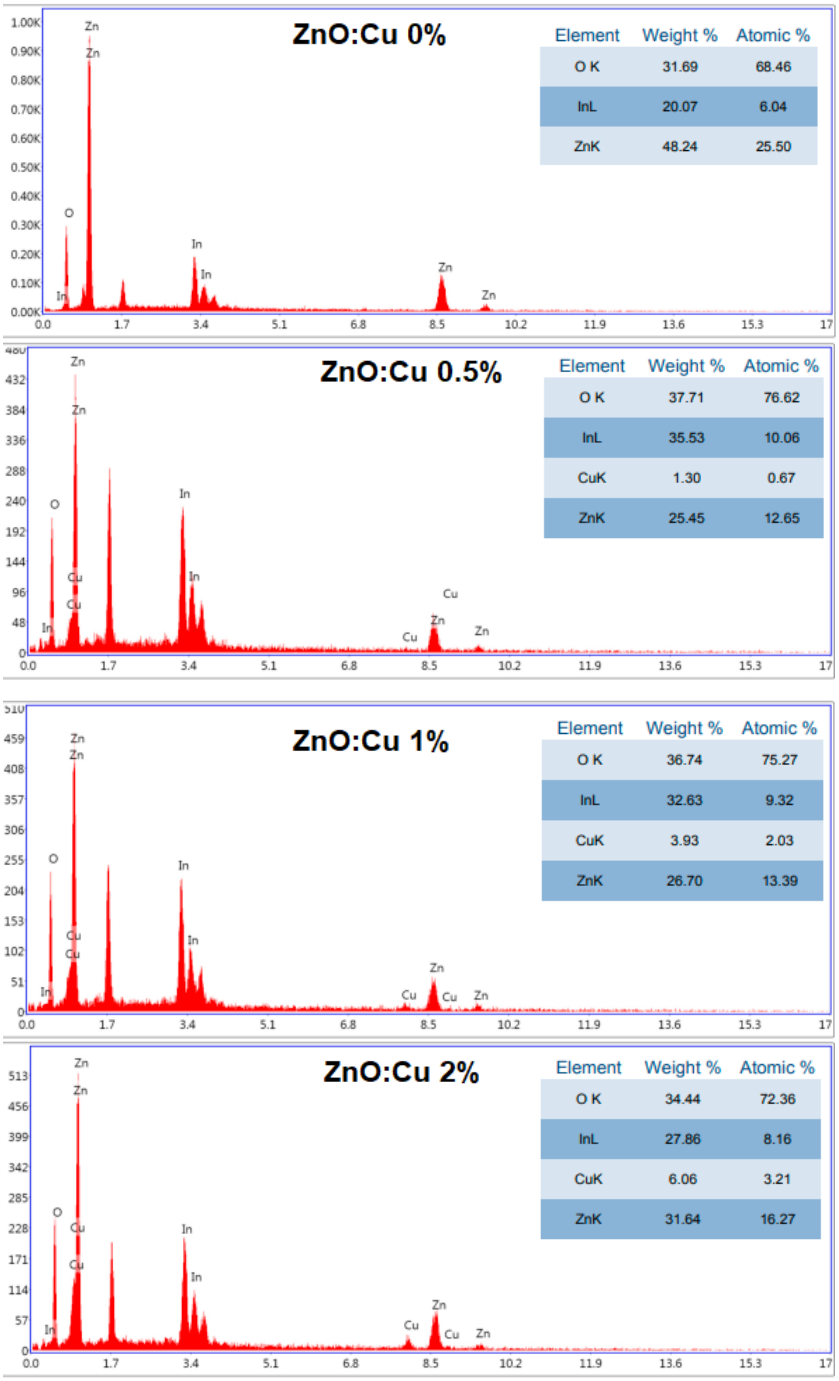

Fig. 3. The EDS spectra of the ZnO:Cu thin films.

Table 2. The EDS analysis of the ZnO:Cu thin films.

Material	Weight (at. %)				O/(Zn+Cu)
	O	Zn	In	Cu	
ZnO:Cu (0%)	31.69	48.24	20.07	-	0.66
ZnO:Cu (0.5%)	37.71	25.54	35.53	1.30	1.40
ZnO:Cu (1%)	36.74	26.70	32.63	3.93	1.20
ZnO:Cu (2%)	34.44	31.64	27.86	6.06	0.91

3.4. Optical characteristics of the ZnO:Cu thin films and ZnO:Cu/H. perforatum structures

The UV–visible optical absorption and transmittance spectra of the ZnO:Cu thin films and ZnO:Cu/*H. perforatum* structure are shown in Fig. 4. The absorption value of pure ZnO thin film and pure ZnO/H. perforatum structure increased slightly with increasing Cu concentration (see Figs. 4(a) and (c)), whereas their transmission spectra decreased (see Figs. 4(b) and (d)). Table 3 shows the transmittance and absorption values of the ZnO:Cu thin films and ZnO:Cu/*H. perforatum* structures.

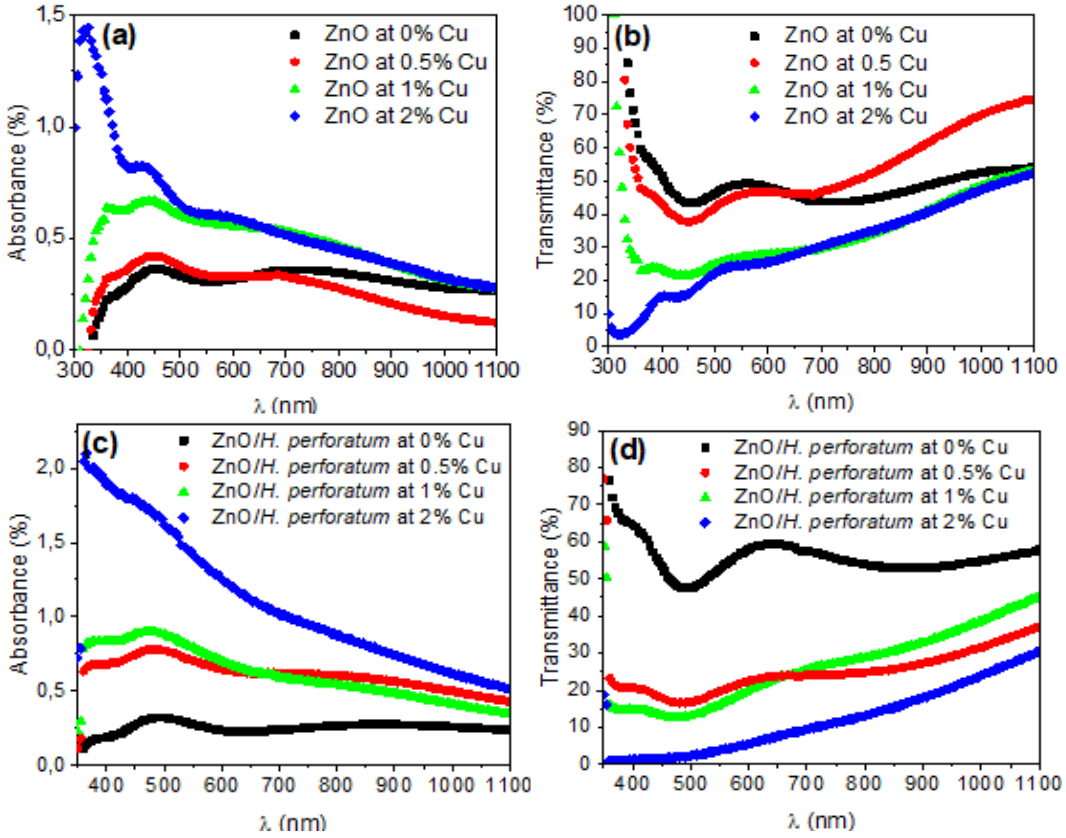

Fig. 4. UV-Vis (a and c) absorption and (b and d) transmission spectra of the ZnO:Cu and ZnO:Cu/H. perforatum thin films with different Cu doping concentrations.

The optical band gap of the ZnO:Cu thin films and ZnO:Cu/*H. perforatum* structure were determined using the Tauc relation [26]. The direct optical band gap energy of the current films was obtained by plotting the $(\alpha h\nu)^2$ vs. ($h\nu$) and extrapolating the linear portion of the absorption edge to find out the intercept with the energy axis (see Fig. 5). Additionally, the optical band gap values of the ZnO:Cu thin films were listed in Table 3, which were quite compatible with the values reported in the literature [23,27]. As can be seen, the band gap of the pure ZnO was 3.75 eV. It had no effect on the Cu concentration of 0.05%. It increased to 3.87 eV for 1% Cu doping and then decreased to 3.08 eV for 2% Cu concentration. Furthermore, the pure ZnO/H. perforatum band gap was determined to be 3.14 eV. For the Cu concentrations of 0.05% and 1%, it stayed at this value, and then it decreased to the value of 2.50 eV for more Cu doping. It is clear that the band gap values of the ZnO:Cu/*H. perforatum* were lower than the ZnO:Cu; that means that adsorption of the *H. perforatum* dye by the ZnO:Cu affects the band gap of the films.

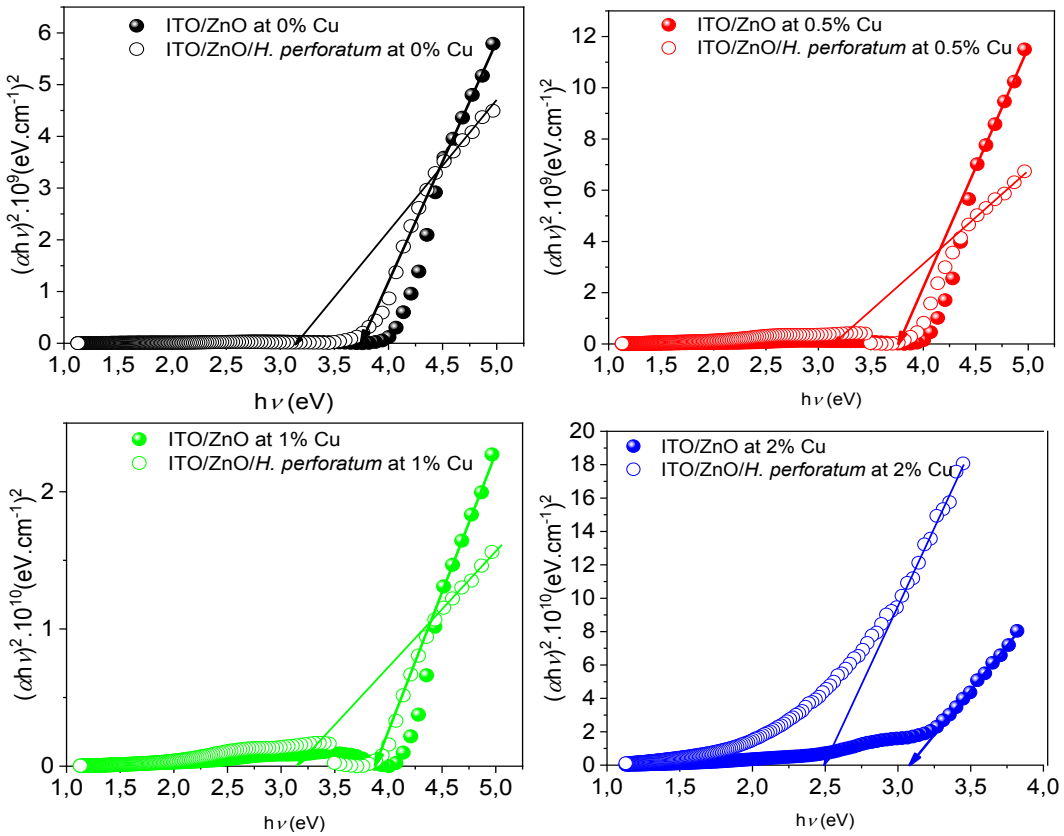

Fig. 5. Plot of $(\alpha h\nu)^2$ vs. $(h\nu)$ for the ZnO:Cu and ZnO:Cu/H. perforatum thin films with different Cu doping concentrations.

Table 3. Thicknesses, and optical properties of the ZnO:Cu and ZnO:Cu/H. Perforatum thin films.

Material	Thickness (nm)	ZnO:Cu			ZnO:Cu/*H. Perforatum*		
		E_g (eV)	A (%) at λ = 500 nm	T (%) at λ = 500 nm	E_g (eV)	A (%) at λ = 500 nm	T (%) at λ = 500 nm
ZnO:Cu (0%)	1619	3.75	0.33	46.30	3.14	0.32	47.60
ZnO:Cu (0.5%)	1090	3.75	0.38	41.90	3.14	0.78	16.80
ZnO:Cu (1%)	672	3.87	0.61	24.80	3.14	0.88	13.10
ZnO:Cu (2%)	615	3.08	0.65	22.20	2.50	1.62	2.40

3.5. The FTIR analysis of the ZnO:Cu thin films

The FTIR measurement was performed to reveal the functional groups in *H. perforatum* dye and ZnO:Cu thin films. The FTIR spectra of *H. perforatum* dye are shown in Fig. 6(a), and the results from the FTIR are listed in Table 4. The bands at 828, 895, and 1018 cm^{-1} would be due to stretching vibration of C–H (trisubstituted alkenes; aliphatic amines) (835–1042 cm^{-1} in Ref. [28]). The band at 1048 cm^{-1} can be assigned to the C–O stretching vibration [29]. Functional groups of esters and lactones (C-O-C) produced an absorption peak at 1154 cm^{-1} (1150-1280 cm^{-1} in Ref. [30]). The bands at 1381 and 1435 cm^{-1} can be assigned to $\delta_s(CH_3)$ (1380–1378 cm^{-1} in [30]) and $\delta(CH_2)$ (1467 cm^{-1} in [30]) bending vibrations due to lin. aliph. chains, respectively. A broad band at 1530 cm^{-1} was due to stretching vibration of ν(the ring) (aromatic ring deformation). This peak observed approximately between 1480 cm^{-1} and 1500 cm^{-1} in Ref. [30] and 1512 cm^{-1} in Ref. [31]. The peaks at 1629 cm^{-1} and 1670 cm^{-1} can be due to the stretching vibrations of the ν(C=C) (1668–1678 cm^{-1}) and ν(C=O) (1650 –

1820 cm^{-1}) bonds in Ref. [30], respectively. These peaks are also observed in the range of 1600–1700 cm^{-1} in Ref. [32]. A band at 1724 cm^{-1} would be related to the ν(C=O) stretching vibration of the carbonyl compound (1650–1820 cm^{-1} in Ref. [30]). The bands at 2838 cm^{-1} (CH_2), 2853 cm^{-1} (CH3), and 2957 cm^{-1} (CH_3) would be due to the vibration of sat. hydrocarbon. These bands are reported at around 2853 cm^{-1}, 2872 cm-1, and 2962 cm^{-1} in Ref [30]. A band at 3030 cm^{-1} can be assigned to the (=C–H), stretching vibration of the cis $R_1HC{=}CHR_2$ group (3010–3030 cm^{-1} in Ref [30]). The presence of the O–H group of polyphenols or polysaccharides (3341 cm^{-1} in Ref. [33]) is demonstrated by the broad band approximately at 3355 cm^{-1}. Additionally, these two bands observed at 3030 cm^{-1} and 3355 cm^{-1} show the presence of anthocyanin in the extract [34]. It can be said that from the FTIR spectra of *H. perforatum* dye, characteristic peaks of polyphenols and biomolecules were observed between 828 cm^{-1} and 3350 cm^{-1} [30].

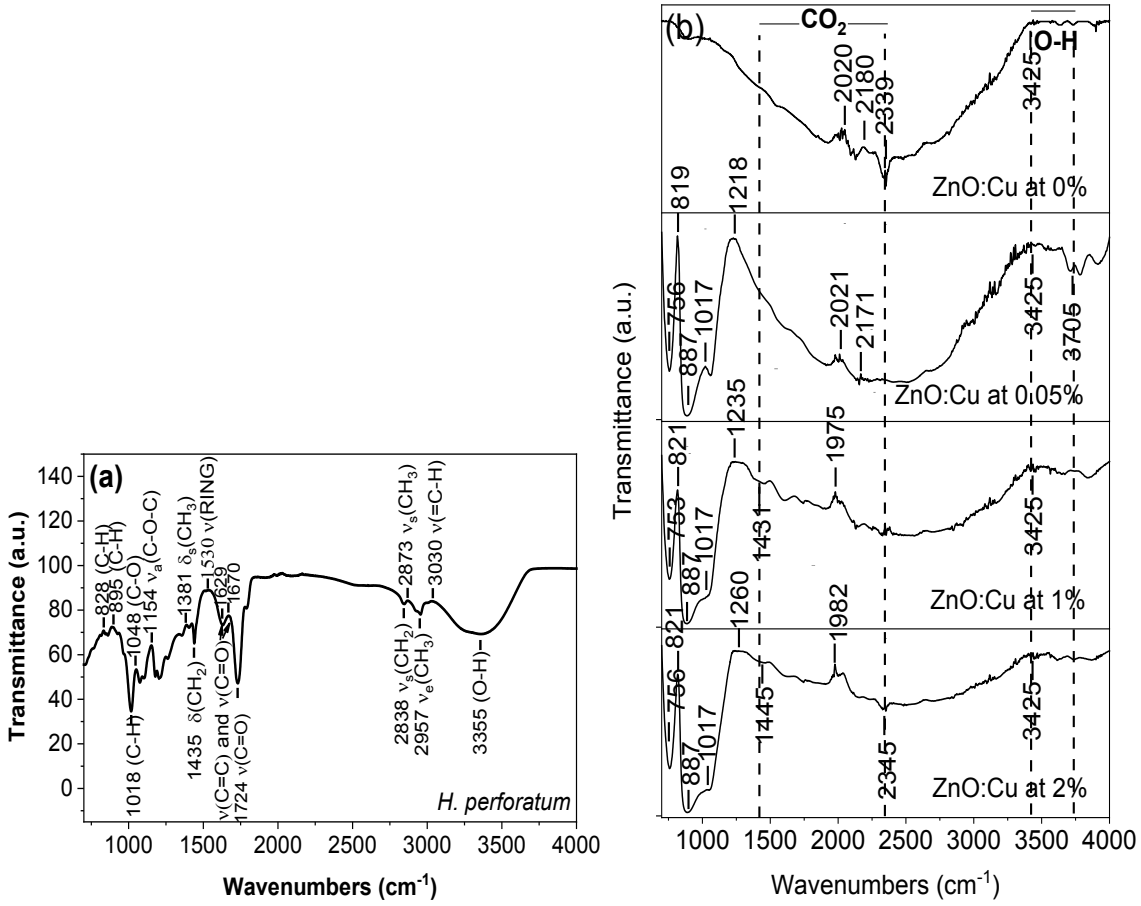

Fig. 6. The FTIR spectra of (a) H. perforatum dye and (b) ZnO:Cu thin films.

Table 4. FTIR analysis of compounds in H. perforatum dye and ZnO:Cu thin films.

Materials	Wave number (cm^{-1})	Type of bond	Ref.
H. perforatum	828-1018	C–H	673-1042 [28]
	1048	C–O	1045-1057 [29]
	1154	ν_a(C–O–C)	1150-1280 [30]
	1381 and 1435	$\delta_s(CH_3)$ and $\delta(CH_2)$	1380-1378 [30] 1467 [28]
	1530	ν(RING)	1480-1500 [30] 1512 [31]
	1629	ν(C=C)	1618-1726 [34] 1668-1678 [30] 1600-1700 [32]
	1670 and 1724	ν(C=O)	1650-1820 [30] 1600-1700 [32]
	2838	$\nu_s(CH_2)$	2853 [30]
	2853	$\nu_s(CH_3)$	2854 [34] 2872 [30]
	2957 cm^{-1}	$\nu_e(CH_3)$	2924 [34] 2962 [30]
	3030	ν(=C–H)	3010-3030 [30]
	3355	O–H	3341 [33] 3336 [34]
ZnO:Cu	1431-2345	CO_2	1396-2360 [30] 2300-2400 [24]
	3425-3705	O-H	3300-3400 [34] 3700 [30] 3455 [24] 3400 [33]

The FTIR spectroscopy has been performed to study the effect of Cu doping on Zn–O bonding. The FTIR spectra of ZnO:Cu thin films are indicated in Fig. 6(b) and tabulated in Table 4. The bands between 753 cm^{-1} and 1260 cm^{-1} are related to the vibrational frequencies arising from the introduction of Cu ions into the ZnO lattice [20,30,35]. Absorption bands observed between 1431-2345 cm^{-1} can be assigned to the absorption of atmospheric CO_2 on the metallic cations [24,28]. The peaks between 3425 cm^{-1} and 3705 cm^{-1} are assigned to the O–H stretching vibration of H_2O in the Cu–Zn–O lattice [24,30,35]. The existence of O–H groups might be due to the adsorption of water molecules on the surface of the ZnO:Cu films because of the method used.

3.6. Photovoltaic performance of the DSSC

The current density-voltage (J-V) characteristics of the DSSC are shown in Fig. 7. Table 5 includes photovoltaic parameters such as J_{SC}, V_{oc}, FF and η are calculated and as well as comparisons with different dyes from the literature. It was observed that a DSSC fabricated using a pure ZnO photoanode showed the highest energy conversion efficiency of 2.47% with 7.66 mA cm^{-2}, 0.98 V, and 329. After introducing Cu^{+2} ions into ZnO, the η of DSSC decreased to 0.38% and then slightly increased to the value of 0.77%. An increase in the power conversion efficiency of DSSCs designed using pure ZnO thin film could be attributed to the mesoporous film surface, as can be seen in Figs. 2 (a) and (e). Mesoporous structure causes the adsorption of more dye molecules onto the ZnO surface, which provides more excited electron injection into the ZnO thin film that leads to an increase in J_{SC} and η. Fig. 7(e) depicts the fabricated DSSC structure.

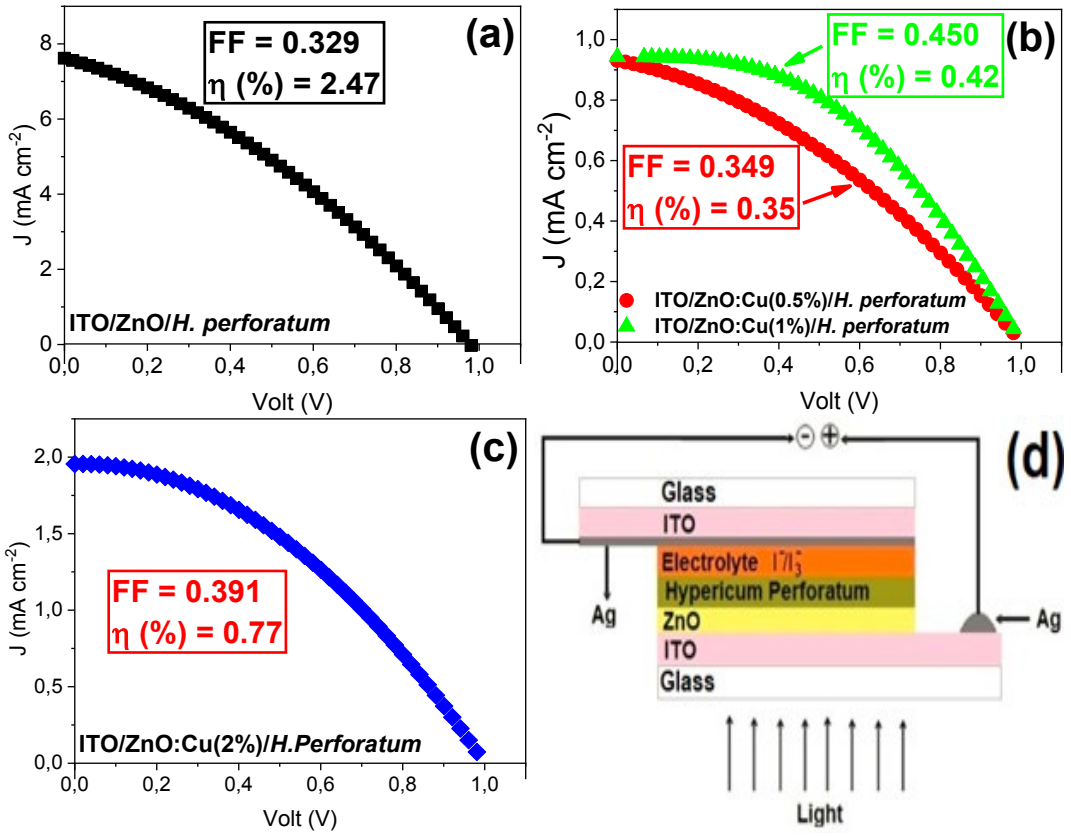

Fig. 6. J-V characteristics of DSSC with different Cu concentrations: (a) Pure (0%), (b) Cu at 0.5% and 1%, and (c) Cu at 2%; (d) structure of a designed DSSC.

Table 5. Photovoltaic performance of ZnO:Cu based DSSCs sensitized with H. perforatum dye and comparison with the previous works.

Natural Dyes	Photo anodes	Electrolyte	V_{oc} (V)	J_{sc} (mA cm^{-2})	*FF*	η (%)
Hibiscus rosa-sinensis	TiO_2-GO	-	0.468	0.039	0.485	0.55 [37]
P. murex	FTO/ZnO	Liquid	0.36	1.16	0.421	0.18% [38]
Tilia Tomentosa	FTO/ZnO	Iodolyte AN-50	0.65	6.26	0.485	1.97 [39]
Delonix regia	ITO/TiO_2	I^-/I_3^-	0.30	1.33	0.390	0.32 [40]
Hibiscus rosasinensis	ITO/ZnO	I^-/I_3^-	0.27	4.20	0.300	0.67 [41]
Linaria	ITOZnO:Cu	I^-/I_3^-	1	0.328	0.640	0.21 [42]
H. perforatum in Ethanol	ITO/ZnO:Cu (0%)	I^-/I_3^-	0.98	7.66	0.329	2.47 (Present work)
H. perforatum in Ethanol	ITO/ZnO:Cu (0.5%)	I^-/I_3^-	1	0.93	0.349	0.38 (Present work)
H. perforatum in Ethanol	ITO/ZnO:Cu (1%)	I^-/I_3^-	1	0.94	0.450	0.42 (Present work)
H. perforatum in Ethanol	ITO/ZnO:Cu (2%)	I^-/I_3^-	1	1.96	0.391	0.77 (Present work)

3. Conclusions

Pure and copper-doped ZnO thin films were synthesized at 85 °C onto ITO substrates using the SILAR method. The XRD analysis of pure ZnO confirmed the formation of a hexagonal wurtzite structure. The intensity of the (100) diffraction peak decreased with increasing Cu doping

concentrations of 0.5%, and it was lost with higher Cu doping concentrations. The surface morphology of the ZnO thin film showed a mixture of spheroid-like and rod-like particles with holes between them. This morphology turned into spherical grains with an increment in Cu doping. The EDS analysis revealed the presence of O, Zn, In, and Cu elements in the films. The bandgap of the pure ZnO film was 3.75 eV. It remained unchanged when 0.05% Cu was added. It increased to a value of 3.87 eV for Cu doping of 1%, and then it decreased to a value of 3.08 eV for Cu doping of 2%. DSSC, which has a simple production process and is low-cost, is produced for the first time by utilizing dye extracted from dried *H. perforatum* flowers. After adsorbing dye molecules, the band gap of the ZnO:Cu thin films decreased. It was 3.12 eV for pure ZnO film, and it stayed the same for Cu-doped ZnO at 0.05% and 1%. Then it decreased to the value of 2.50 eV for Cu doped at 2%. The FTIR spectra indicated the existence of several functional groups in the *H. perforatum* dye and ZnO:Cu thin films. The J-V characteristics of the present DSSC were measured, and the photovoltaic parameters were investigated.

In summary, Cu doping in ZnO lattice significantly changed the structural, morphological, compositional, and optical properties of the ZnO thin films. However, it did not increase the performance of DSSC. The highest energy conversion efficiency was 2.47% for the DSSC synthesized with pure ZnO in the structure of glass/ITO/ZnO/*H. perforatum*/electrolyte/ITO/glass. A DSSC obtained using pure ZnO thin film has the appropriate physical properties and cell efficiency to be applied as a photoanode on a DSSC.

References

[1] B. O'Regan, M. Grätzel, Nature, 353, 737 (1991); https://doi.org/10.1038/353737a0

[2] M. Grätzel, Inorg. Chem., 44(20), 6841 (2005); https://doi.org/10.1021/ic0508371

[3] K. Obi, L. Frolova, P. Fuierer, Sol. Energy, 208, 312 (2020); https://doi.org/10.1016/j.solener.2020.08.006

[4] M.Y. Hsieh, F.I. Lai, W.C. Chen, M.C. Hsieh, H.Y. Hu, P. Yu, H.C. Kuo, S.Y. Kuo, Nanoscale, 8(10), 5478 (2016); https://doi.org/10.1039/C5NR07948A

[5] P. Sanjay, I. Isaivani, K. Deepa, J. Madhavan, S. Senthil, Mater. Lett., 244, 142 (2019); https://doi.org/10.1016/j.matlet.2019.02.072

[6] H.K. Reshma, B.S. Avinash, V.S. Chaturmukha, R.L. Ashok, H.S. Jayanna, Mater. Today: Proc., 37, 434 (2021); https://doi.org/10.1016/j.matpr.2020.05.424

[7] M. Grätzel, J. Photochem. Photobiol. A: Chemistry, 164, 1-3 (2004); https://doi.org/10.1016/j.jphotochem.2004.02.023

[8] S.G. Ullattil, P. Periyat, Sol. Energy, 147 99 (2017); https://doi.org/10.1016/j.solener.2017.03.039

[9] P. Sanjay, K. Deepa, J. Madhavan, S. Senthil, Opt. Mater., 83, 192 (2018); https://doi.org/10.1016/j.optmat.2018.06.011

[10] S. Singh, A. Singh, N. Kaur, Bull. Mater. Sci., 39, 1371 (2016); https://doi.org/10.1007/s12034-016-1283-y

[11] D. Kumbhar, S. Delekar, S. Kumbhar, A. Dhodamani, N. Harale, R. Nalawade, A. Nalawade, Chem. Pap., 75, 4019 (2021); https://doi.org/10.1007/s11696-021-01658-z

[12] M. Makenali, I. Kazeminezhad, Mater. Res. Innov., 25(7), 387 (2021); https://doi.org/10.1080/14328917.2020.1831144

[13] B.G Zhai, L. Yang, Y.M. Huang, Mater. Res. Innov., 19(7), 15 (2015); https://doi.org/10.1179/1432891715Z.0000000002045

[14] M. Sathya, G. Selvan, K. Kasirajan, S. Usha, P. Baskaran, M. Karunakaran, S.S.R. Inbanathan, Braz. J. Phys., 52, 23 (2022); https://doi.org/10.1007/s13538-021-01026-y

[15] M.U. Özbek, M. Koç, E. Hamzaoğlu, Turk. J. Bot., 43(5), 694 (2019); https://doi.org/10.3906/bot-1902-27

[16] S.L. Crockett, N.K.B. Robson, Med. Aromat. Plant Sci. Biotechnol., 5(1), 1 (2011); PMID: 22662019

[17] A. Güner, S. Aslan, T. Ekim, M. Vural, M.T. Babaç, (edlr.), Türkiye Bitkileri Listesi (Damarlı

Bitkiler), Nezahat Gökyiğit Botanik Bahçesi ve Flora Araştırmaları Derneği Yayını, İstanbul (2012).
[18] E. Ersoy, E.E. Ozkan, M. Boga, A. Mat, Evaluation of in vitro biological activities of three Hypericum species (H. calycinum, H. confertum, and H. perforatum) from Turkey. S. Afr. J. Bot., 130, 141-147 (2020); https://doi.org/10.1016/j.sajb.2019.12.017
[19] A.K. Ayan, C. Çirak, Hypericin and Pseudohypericin contents in some Hypericum species growing in Turkey, Pharm. Biol., 46(4), 288-291 (2008); https://doi.org/10.1080/13880200701741211
[20] C. Çırak, A. Bertoli, L. Pistelli, F. Seyis, Essential oil composition and variability of Hypericum perforatum from wild populations of northern Turkey, Pharm. Biol., 48(8) 906-914 (2010); https://doi.org/10.3109/13880200903311136
[21] F. Göde, S. Ünlü, Mater. Sci. Semicon. Proc., 90, 92 (2019); https://doi.org/10.1016/j.mssp.2018.10.011
[22] N. Balpınar, F. Göde, Fabrication and characterization of dye-sensitized solar cells based on murexid dye and inorganic CdS:mn thın fılms, Chalcogenide Lett. 17, 429 (2020)
[23] C. Gumus, O.M. Ozkendir, H. Kavak, Y. Ufuktepe, J. Optoelectron. Adv. M., 8(1), 299 (2006)
[24] S. Muthukumaran, R. Gopalakrishnan, Opt. Mater., 34(11), 1946 (2012); https://doi.org/10.1016/j.optmat.2012.06.004
[25] Göde, F.; Ünlü, S. Open Chem., 16, 757-762 (2018); https://doi.org/10.1515/chem-2018-0089
[26] J. Tauc, Amorphous and Liquid Semiconductors, Plenum Press, New York (1974); https://doi.org/10.1007/978-1-4615-8705-7
[27] E. Güneri, B. Stadler, MRS. Commun., 9(3), 1105 (2019); https://doi.org/10.1557/mrc.2019.82
[28] T. Abodunrin, A. Boyo, O. Obafemi, T. Adebayo, Mater. Sci. Appl., 6(7), 646-655 (2015); https://doi.org/10.4236/msa.2015.67066
[29] R. Ramanarayanan, P. Nijisha, C.V. Niveditha, S. Sindhu, Mater. Res. Bull. 90, 156-161 (2017); https://doi.org/10.1016/j.materresbull.2017.02.037
[30] B. Schrader, Infrared and Raman Spectroscopy: Methods and Applications, VCH Publisher, New York, 1995; https://doi.org/10.1002/9783527615438
[31] J.R. Franca, M.P. De Luca, T.G. Ribeiro, R.O. Castilho, A.N. Moreira, V.R. Santos, A.A. Faraco, BMC Complement. Altern. Med., 14, 478 (2014); https://doi.org/10.1186/1472-6882-14-478
[32] M. Heydarian, H. Jooyandeh, B. Nasehi, M. Noshad, M. Int. J. Biol. Macromol., 104, 287 (2017); https://doi.org/10.1016/j.ijbiomac.2017.06.049
[33] S.A. Khan, F. Noreen, S. Kanwal, A. Iqbal, G. Hussain, Mater. Sci. Eng. C 82, 46 (2018); https://doi.org/10.1016/j.msec.2017.08.071
[34] P. Sanjay, I. Isaivani, K. Deepa, J. Madhavan, S. Senthil, S, Mater. Lett., 244, 142 (2019); https://doi.org/10.1016/j.matlet.2019.02.072
[35] D. Sahu, N.R. Panda, B.S. Acharya, A.K. Panda, Ceram. Int., 40(7), 11041 (2014); https://doi.org/10.1016/j.ceramint.2014.03.119
[36] P. Sanjay, K. Deepa, J. Madhavan, S. Senthil, Mater. Lett., 219, 158 (2018); https://doi.org/10.1016/j.matlet.2018.02.085
[37] K. Mensah-Darkwa, F.O. Agyemang, D. Yeboah, S. Akromah, Mater. Today: Proc., 38, 514 (2021); https://doi.org/10.1016/j.matpr.2020.02.391
[38] T. Marimuthu, N. Anandhan, T. Mahalingam, R. Thangamuthu, M. Mummoorthi, J. Mater. Sci.: Mater. Electron, 26(10), 7577 (2015); https://doi.org/10.1007/s10854-015-3394-4
[39] R. Shashanka, H. Esgin, V.M. Yilmaz, Y. Caglar, J. Sci.: Adv. Mater. Devices, 5, 185 (2020); https://doi.org/10.1016/j.jsamd.2020.04.005
[40] T.S. Senthil, N. Muthukumarasamy, D. Velauthapillai, S. Agilan, M. Thambidurai, R. Balasundaraprabhu, Renew. Energy, 36(9), 2484 (2011); https://doi.org/10.1016/j.renene.2011.01.031
[41] M. Thambidurai, N. Muthukumarasamy, D. Velauthapillai, C. Lee, Mater. Lett. 92, 104 (2013); https://doi.org/10.1016/j.matlet.2012.10.036
[42] N. Balpınar, Emerg. Mater. Res., 11(4), 1-10 (2022); https://doi.org/10.1680/jemmr.22.00073